Binary mixed homopolymer brushes grafted on nanorod particles: A self-consistent field theory study

Xin Ma, Yingzi Yang, Lei Zhu, Bin Zhao, Ping Tang, and Feng Qiu

Articles you may be interested in

Ordered structures of diblock nanorods induced by diblock copolymers
J. Chem. Phys. **139**, 104901 (2013); 10.1063/1.4819775

Synthesis and characterization of PMMA- ZrO 2 nanocomposites
AIP Conf. Proc. **1536**, 187 (2013); 10.1063/1.4810163

Organic bistable memory based on Au nanoparticle/ZnO nanorods composite embedded in poly (vinylpyrrolidone) layer
Appl. Phys. Lett. **99**, 023303 (2011); 10.1063/1.3605596

Mixed homopolymer brushes grafted onto a nanosphere
J. Chem. Phys. **134**, 134903 (2011); 10.1063/1.3575180

Nanoparticulate AlO (OH) n filled polyvinylidenefluoride-co-hexafluoropropylene based microporous membranes for lithium ion batteries
J. Renewable Sustainable Energy **1**, 023108 (2009); 10.1063/1.3122671

Binary mixed homopolymer brushes grafted on nanorod particles: A self-consistent field theory study

Xin Ma,[1] Yingzi Yang,[1] Lei Zhu,[2] Bin Zhao,[3] Ping Tang,[1,a)] and Feng Qiu[1,a)]

[1]*Department of Macromolecular Science, The State Key Laboratory of Molecular Engineering of Polymers, Key Laboratory of Computational Physical Sciences, Fudan University, Shanghai 200433, China*
[2]*Department of Macromolecular Science and Engineering, Case Western Reserve University, Cleveland, Ohio 44106-7202, USA*
[3]*Department of Chemistry, University of Tennessee, Knoxville, Tennessee 37996, USA*

We employ the self-consistent field theory to study phase structures of brush-rod systems composed of two chemically distinct linear homopolymers. The polymer chains are uniformly grafted on the surface of a nanorod particle of finite length and comparable radius to the polymer radius of gyration. A "masking" technique treating the cylindrical boundary is introduced to solve the modified diffusion equations with an efficient and high-order accurate pseudospectral method involving fast Fourier transform on an orthorhombic cell. A rich variety of structures for the phase separated brushes is predicted. Phase diagrams involving a series of system parameters, such as the aspect ratio of the nanorod, the grafting density, and the chain length are constructed. The results indicate that the phase structure of the mixed brush-rod system can be tailored by varying the grafted chain length and/or the aspect ratio of the rod to benefit the fabrication of polymeric nanocomposites. © 2013 AIP Publishing LLC. [http://dx.doi.org/10.1063/1.4832742]

I. INTRODUCTION

Due to their tunable chemical properties and sensitive response to environmental stimulus, surface-confined macromolecules known as polymer brushes have broad potential applications in a variety of areas, such as colloidal stabilization, tuning of the adhesion and wetting properties of surface, coatings preventing or preferring biological systems, etc.[1–3] A variation of polymer brushes, mixed polymer brushes, has attracted tremendous interest in recent years.[4,5] When chemically distinct linear chains are grafted on the substrate, the physical (such as brush height and roughness) and chemical properties (such as hydrophobicity and hydrophilicity), as well as the morphology can be delicately designed by adjusting a large space of system parameters including solvent selectivity,[6–10] degree of polymerization,[6,8–13] grafting position and density,[6,8,12,14] geometry of the substrate surface,[1,3,15–17] etc.

Depending on the balance between the stretching of chain configuration and the binary interactions between different components, mixed polymer brushes can only undergo microphase separation leading to well-defined nanostructures. The early theoretical work on mixed polymer brushes by Marko and Witten[18,19] studied the equilibrium phase morphology of binary mixed brushes grafted on a planar substrate and predicted a transition from miscible state to ripple phases. In the recent two decades, the invention of "graft to" and "graft from" methods enables the fabrication of polymer brushes with well controlled thickness and a high degree of grafting density to approximately one chain per square nanometer,[4,7–9,20–22] and thus abundant theoretically predicted phase morphologies for binary mixed brushes anchoring on a flat plane, such as ripple, dimple, layer, and micelles,[7,14,18,19,25] are possible to be achieved experimentally.

Polymer brushes grafted on particles with a finite surface area have great potential for applications.[5] On one hand, the brushes can be engineered to combine desired properties of both core particles and polymer brushes to fulfill the requirements from nanotechnology.[1,5] On the other hand, when the substrate is finite, the morphology of binary mixed brushes must cope with the substrate geometry. This promises abundant potential nanostructures. However, despite the knowledge on the most frequently studied planar brushes,[4,6–9,14,18–26] the study of polymer brushes (especially mixed polymer brushes) on the surface of spherical colloids or nanoparticles is limited.[5,10–13,15–17,27–30]

Mixed polymer brushes grafted on particles, especially on a spherical core, are prospected as a new class of environmentally responsive nano-materials, which can be designed as Janus particles or multi-valent colloidal particles with distinct functions of different domains.[5] Roan[11,12] predicted that the binary mixed brushes exhibit a sequence of ripple, island, and layer phases by increasing the difference in the chain numbers (or grafting densities) and the chain lengths of the two species. In our previous work,[13] we explored the morphology of spherical mixed brushes with a large space of system parameters, and established phase diagrams with a rich variety of phases. We found a series of island structures with different island numbers representing specific structure symmetry in contrast to conventional hexagonal arrangement. The spherical particle radius plays a significant role in determining the type of the island structures.

a)Authors to whom correspondence should be addressed. Electronic addresses: pingtang@fudan.edu.cn and fengqiu@fudan.edu.cn

On a cylindrical substrate, the asymmetric surface curvature may introduce interesting phase behaviors. For both planar and spherical surfaces, the curvature at each position on the surface is identical; therefore, preference of different morphology orientations is lost. However, when the substrate is elongated, such as a cylindrical rod, the chain extensions in the radial, axial, and lateral directions are different due to the asymmetric curvatures in different directions along the substrate.[30]

Although the synthesis of covalently grafted brushes on a cylindrical core is already technically possible,[29] there is, to our knowledge, no theoretical or experimental study on the mixed homopolymer brushes with immobile ends grafted on a cylindrical surface at present. Nevertheless, brushes with mobile grafting sites,[15–17] or physically absorbed polymers on a rod have been reported.[26] Interestingly, in such systems allowing macrophase separation, a ripple phase composed of ring-shaped alternating stripes perpendicular to the cylinder axis is proved, experimentally as well as theoretically,[15–17] to be a meta-stable phase.

Among a variety of theoretical and simulation methods, such as scaling method,[3,6,30–32] molecular dynamics,[33] density functional theory,[23] and dissipative particle dynamics (DPD),[15,16] the self-consistent-field theory (SCFT) is one of the most important and frequently used approaches to make accurate prediction for the morphology of polymer brushes.[7,11–14,17,25–27] In our previous work, we have developed a spherical alternating-direction implicit scheme to numerically solve SCFT in real-space for investigating the self-assembly of block copolymers on spherical surface.[34] The major problem of numerically solving diffusion equations on closed surfaces is the "pole problem." Recently, we have numerically solved the diffusion equations with SCFT by employing a so-called "masking" technique for polymer grafted on a substrate,[13,35] which enables us to calculate with arbitrary geometrical shape. In this paper, we extend this method to the cylindrical brush system.

The remainder of the paper is organized as follows. We start with a description of the mixed brush-rod system and then briefly summarize the SCFT approach in Sec. II. Then the results for the phase separated mixed brush-rod system immersed in a neutral solvent are described in Sec. III. Finally, the conclusions are summarized in Sec. IV.

II. THEORETICAL MODEL

We construct our polymer brushes by homogeneously and covalently grafting two kinds of linear homopolymers A and B on a cylindrical nanoparticle, and immerse the system in a solvent S. The Kuhn length of polymers $b_A = b_B = b$ equals unit, and the volume of a polymer segment and of a solvent molecule is $v_A = v_B = v_S = \rho_0^{-1} = b^3$. The volume fraction of component i is defined as $c_i = n_i N_i v_i / \sum_{i=A,B,S} n_i N_i v_i$, where n_i is the number of molecules of component i, and N_i is the number of segments of one molecule of component i. The ratios of the relative chain length for A and B are defined as $\alpha_A = N_A/N$ and $\alpha_B = N_B/N$, respectively, where the reference N is chosen to be N_A. N_S is set to be one. The Flory-Huggins interaction pa-
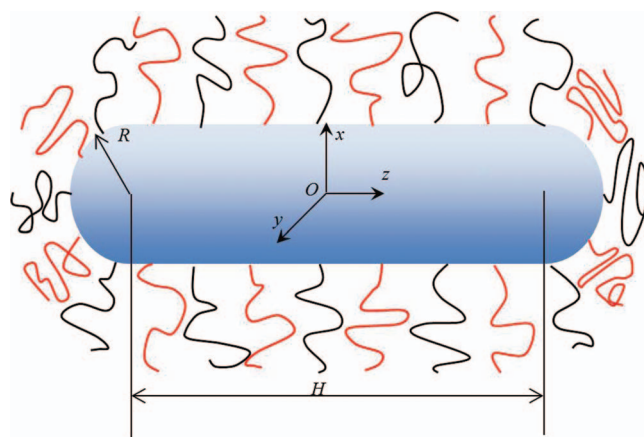

FIG. 1. A scheme of the cross section of *xz*-plane of the binary mixed brush-rod model. The black and the red curves represent the homopolymers A and B grafted on the surface of the nanorod core, respectively.

rameter between species i and j is denoted as χ_{ij} ($i, j = $ A, B, S, or W, here W means rod surface). The local volume fractions of species i is $\phi_i(\mathbf{r})$, which obeys the incompressibility constrain,

$$\phi_A(\mathbf{r}) + \phi_B(\mathbf{r}) + \phi_S(\mathbf{r}) + \phi_W(\mathbf{r}) = 1. \quad (1)$$

The nanorod, which is the core of the brush-rod system, has a cylindrical region of length H and radius R, and a hemispherical cap of radius R at both ends (Fig. 1). The cylinder axis is chosen to be *z*-axis. The center of the nanorod is placed at the coordinate origin O. Since the polymer is uniformly grafted on the surface of the nanorod, the grafting density is calculated to be $\sigma_i = \frac{n_i}{2\pi R H + 4\pi R^2}$ ($i = $ A or B).

We employ SCFT to calculate the phase morphology and the free energy of the system.[36–39] The free energy of the whole system is given as

$$\frac{F}{k_B T} = \frac{\rho_0}{N} \int d\mathbf{r} \left\{ \frac{1}{2} \sum_{i \neq j} \chi_{ij} N \phi_i(\mathbf{r}) \phi_j(\mathbf{r}) - \sum_k \omega_k(\mathbf{r}) \phi_k(\mathbf{r}) \right.$$
$$\left. - \xi(\mathbf{r}) \left(1 - \sum_i \phi_i(\mathbf{r}) \right) \right\}$$
$$- \sum_k n_k \ln Q_k \quad (2)$$

$$i, j = \text{A, B, S or W}, \quad k = \text{A, B or S},$$

where $\omega_A(\mathbf{r})$, $\omega_B(\mathbf{r})$, and $\omega_S(\mathbf{r})$ are the conjugated potentials, and $\xi(\mathbf{r})$ is the Lagrange multiplier which enforces the incompressibility constraint. By minimizing Eq. (2) with respect to $\phi_i(\mathbf{r})$ and $\omega_i(\mathbf{r})$, the self-consistent equations of the brush-rod system are obtained as[13]

$$\omega_A(\mathbf{r}) = \chi_{AB} N \phi_B(\mathbf{r}) + \chi_{AS} N \phi_S(\mathbf{r}) + \chi_{AW} N \phi_W(\mathbf{r}) + \xi(\mathbf{r}), \quad (3)$$

$$\omega_B(\mathbf{r}) = \chi_{AB} N \phi_A(\mathbf{r}) + \chi_{BS} N \phi_S(\mathbf{r}) + \chi_{BW} N \phi_W(\mathbf{r}) + \xi(\mathbf{r}), \quad (4)$$

$$\omega_S(\mathbf{r}) = \chi_{AS} N \phi_A(\mathbf{r}) + \chi_{BS} N \phi_B(\mathbf{r}) + \chi_{SW} N \phi_W(\mathbf{r}) + \xi(\mathbf{r}), \quad (5)$$

$$\phi_A(\mathbf{r}) = \frac{c_A}{Q_A \alpha_A} \int_0^{\alpha_A} ds\, q_A(\mathbf{r}, s) q_A^+(\mathbf{r}, \alpha_A - s), \qquad (6)$$

$$\phi_B(\mathbf{r}) = \frac{c_B}{Q_B \alpha_B} \int_0^{\alpha_B} ds\, q_B(\mathbf{r}, s) q_B^+(\mathbf{r}, \alpha_B - s), \qquad (7)$$

$$\phi_S(\mathbf{r}) = \frac{c_S}{Q_S} \exp(-\omega_S(\mathbf{r})/N), \qquad (8)$$

where the polymer chain is parameterized with a continuous path variable s.

The so-called "masking" technique, which was originally proposed by Khanna *et al.*,[40] is employed to deal with the confined polymers grafted onto the curved surface. We have developed a method to solve the morphology of block copolymers confined into complicated topographic surfaces with SCFT.[13,35] In this paper, this unique technique is extended to solve the SCFT for nanorod grafted by mixed polymer brushes. The details of this technique can be found in Refs. 13 and 35. In this way, the use of simple Cartesian grids in a cubic computational cell with periodic boundary conditions makes it possible to solve diffusion equations in SCFT by utilizing an efficient and highly accurate pseudo-spectral method involving fast Fourier transformation, which was first developed by Tzeremes *et al.*[41] The "cavity" field $\phi_W(\mathbf{r})$ to smooth the boundary condition is defined as

$$\phi_W(\mathbf{r}) = \begin{cases} 1.0 & r_c \leq 0 \\ \frac{1}{2}\left\{1 - \tanh\left[\frac{m}{t}\left(r_c - \frac{T}{2}\right)\right]\right\} & r_c > 0 \end{cases}, \qquad (9)$$

where

$$r_c = \begin{cases} \sqrt{r_x^2 + r_y^2 + (r_z + H/2)^2} - R, & r_z < -H/2 \\ \sqrt{r_x^2 + r_y^2} - R, & -H/2 \leq r_z \leq H/2 \\ \sqrt{r_x^2 + r_y^2 + (r_z - H/2)^2} - R, & r_z > H/2 \end{cases} \qquad (10)$$

is the distance between a position $\mathbf{r} = (r_x, r_y, r_z)$ and its nearest position on the surface of the rod. The positive or negative value of r_c implies $\mathbf{r}$ inside and outside the rod, respectively. $r_c = 0$ denotes the positions on the nanorod surface. In this work, the constants in Eq. (9) are $m = 4.60$, $t = 1.0$, $T = 2.5$, and $R_g = 0.5N^{1/2}b$.

In Eqs. (6) and (7), the propagator $q_i(\mathbf{r}, s)(i = A \text{ or } B)$ corresponds to the probability of finding a partial polymer chain i of length s that starts from $s = 0$ anywhere in the system and ends at position $\mathbf{r}$, where the chain contour length $s \in [0, \alpha_i]$. It satisfies the diffusion equation,

$$\frac{\partial q_i(\mathbf{r}, s)}{\partial s} = \frac{Nb^2}{6} \nabla^2 q_i(\mathbf{r}, s) - \omega_i(\mathbf{r}) q_i(\mathbf{r}, s), \quad i = A \text{ or } B, \qquad (11)$$

with the boundary condition,

$$q_i(\mathbf{r}, 0) = \begin{cases} 1, & r_c > 0 \\ 0, & r_c \leq 0 \end{cases}, \quad i = A \text{ or } B. \qquad (12)$$

Similarly, another propagator $q_i^+(\mathbf{r}, s)$ corresponds to the probability for a partial polymer chain i of length s that starts from the grafting end of the chain and ends at position $\mathbf{r}$. $q_i^+(\mathbf{r}, s)$ satisfies the same diffusion equation as Eq. (11). A

different boundary condition has to be applied for uniform grafting,

$$q_i^+(\mathbf{r}, 0) = \begin{cases} \frac{\sigma_i}{q_i(\mathbf{r}, \alpha_i)}, & r_c \in (0, b) \\ 0, & r_c \notin (0, b) \end{cases}, \quad i = A \text{ or } B. \qquad (13)$$

Therefore, the chains are grafted within a quite small distance of Kuhn length b above the surface of the nanorod and the effective grafting density is

$$\sigma_i' = \frac{n_i}{4\pi(R+b)^2 + 2\pi(R+b)H}, \quad i = A \text{ or } B. \qquad (14)$$

Previously, a similar treatment to improve the numerical stability has been introduced by Kim and Matsen.[27]

We use the pseudo-spectral method to solve the diffusion equation in a cubic box subjected to periodic boundary conditions.[41,42] The main advantage of this method is its ability to treat domain of arbitrary geometrical shape in contrast to finite-difference and finite element methods. Therefore, the discretized form of the diffusion equation is

$$q_i(\mathbf{r}, s + \Delta s) = \exp\left[-\frac{\Delta s}{2}\omega_i(\mathbf{r})\right] \exp\left[\frac{Nb^2}{6}\Delta s \nabla^2\right]$$
$$\times \exp\left[-\frac{\Delta s}{2}\omega_i(\mathbf{r})\right] q_i(\mathbf{r}, s). \qquad (15)$$

Compared with the real-space solution of the diffusion equation, the pseudo-spectral method involving fast Fourier transformation is more efficient and accurate.[41]

The single chain partition functions Q_A and Q_B for homopolymers A and B, and the partition function Q_S for solvent S, are calculated via equations

$$Q_A = \frac{1}{V} \int d\mathbf{r}\, q_A^+(\mathbf{r}, \alpha_A), \qquad (16)$$

$$Q_B = \frac{1}{V} \int d\mathbf{r}\, q_B^+(\mathbf{r}, \alpha_B), \qquad (17)$$

$$Q_S = \frac{1}{V} \int d\mathbf{r} \exp[-\omega_S(\mathbf{r})/N], \qquad (18)$$

where $V = \int d\mathbf{r}(1 - \phi_W(\mathbf{r}))$ represents the effective volume occupied by polymer and solvent.

III. RESULTS AND DISCUSSION

The mixed brush-rod system can be fabricated by different methods.[4] The covalent attachment can be accomplished by either "grafting to" (end-functionalized chains react with an appropriate substrate) or "grafting from" (polymer chains are grown from the initiator immobilized on the substrate) approaches. The "grafting from" approach is more promising for the fabrication of polymer brushes with a high grafting density;[4,8] the thickness, grafting density, and molecular weight of the grafted polymer chains can be regulated by grafting time, monomer concentration, initiator density, etc. Therefore, in the SCFT calculation, we assume all these system parameters are respectively controllable.

To reduce the parameter space, we assume both the nanorod and the solvent are neutral to A and B homopolymers, i.e., the Flory-Huggins parameters $\chi_{AS} = \chi_{BS} = \chi_{AW}$

$= \chi_{BW} = \chi_{SW} = 0$. We choose the chain length $N_A + N_B = 48$. The calculations are carried out in a three-dimensional space of $Lx \times Ly \times Lz$ lattice, with the spatial discretization $\Delta x = \Delta y = \Delta z = 0.25b$. The chain contour is discretized with a step length $\Delta s = b/30$. The radius of the cylindrical region of the nanorod is fixed to be $R = 3b$, and the aspect ratio of the nanorod is denoted as $\varepsilon = (H + 2R)/2R$, with $\varepsilon = 1$ for spherical core and $\varepsilon > 1$ for elongated rod. The total grafting density in all of our calculations is fixed to be $\sigma = \sigma_A + \sigma_B = 0.6b^{-2}$, which locates in the high grafting density region where chains are contacting each other and are strongly stretching out near the substrate. The polymer chains are densely tethered by one end via a covalent bond onto the core surface. So that the grafting segments are immobile, thus only microscopic phase separation can occur.

We define the relative volume fraction of component A as $f_A = c_A/(c_A + c_B) = \sigma_A N_A/(\sigma_A N_A + \sigma_B N_B)$, which is a function of the chain length N_A and N_B, and also is a function of grafting density σ_A and σ_B.

Our coarse-grained parameters can be translated into physical dimensions as follows. Taking the experimentally well-established mixed poly(tert-butyl acrylate) (PtBA)/PS brushes grafted on silica particles as an example,[5] the Kuhn length for PS is around $b = 1.8$ nm, thus for a typical chain length chosen in this paper, $N = 24$, the chain contour length is 43.2 nm and the end-to-end distance is 8.8 nm. The radius of the cylinder we chose is $R = 3b = 5.4$ nm and its length H varies from 0 to 32.4 nm. The total grafting density is around 0.2 chain/nm^2. These are all synthetically reasonable values.[5]

A. Symmetric brushes

We define $\sigma_A = \sigma_B$ and $N_A = N_B$ as the symmetric mixed brushes. Therefore, the relative volume fractions are $f_A = f_B = 0.5$. Such symmetric brushes could be fabricated by connecting different copolymer chains on each branch of a delicately designed Y-shaped initiator covalently grafted on the substrate.[9,22]

1. Morphology

When the polymer brushes are grafted on a spherical core (corresponding to $\varepsilon = 1$), a typical ripple structure with two spiral domains is obtained (as shown in Fig. 2(a)). The morphology has D_1 symmetry for each domain, and has D_2 symmetry for geometry with different colors. Therefore, domain A can overlap with domain B if the brushes rotate with respect to the spiral axis by an angle π. Such ripple structure was also observed in Roan's work,[12] and in our previous study.[13] However, the spiral structure is not stable when the core is slightly elongated ($\varepsilon = 1.5$, Fig. 2(b1)).

When $\varepsilon > 1$, we find that ripple structures perpendicular (ring-shaped) and parallel to the rod axis are both possible (they are both the solution of the self-consistent equations with slight different free energies). It turns out that the free energy of the system is mainly determined by the entropy of the solvent, which means a slight change of the solvent selectivity could reverse the relative stability of the perpendicular
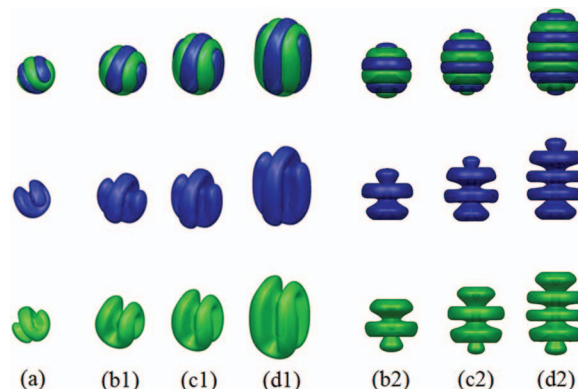

FIG. 2. Typical morphologies of the symmetric brush-rod systems ($\chi_{AB}N = 40$) with $\varepsilon = 1$, 1.5, 2.5, 4 from (a) to (d1)/(d2). The numbers 1 and 2 represent R$_4$ and 4-Rin morphologies at the same ε, respectively. The second and third rows are domains A and B drawn with $\phi_A \geq c_A$ and $\phi_B \geq c_B$, respectively. The morphologies in the first row are the combination of that in the second and third rows.

and parallel ripple structures. In present calculation, we have assumed a perfect neutral solvent ($\chi_{AS} = \chi_{BS} = 0$) for simplicity, while in reality for two specific polymers any solvent always prefers one of the polymer – no matter how weak is the selectivity. Therefore to better compare the experiment, we present and discuss the structures of both perpendicular and parallel ripple phases (Fig. 2). The parallel ripple phase is denoted as R$_n$, where n is the number of periods of the density profile of one component in the equator plane $z = 0$. The perpendicular ripple phase or the ring-shaped phase is denoted as n-Rin, where n is the number of periods of the density profile of one component in the plane that includes the rod axis.

Taking R$_4$ as an example, the domains for components A and B have different configuration although the parameter settings are symmetric (Fig. 2(b1)). One component forms a continuous matrix (domain B in Fig. 2(b1)), while the other one (domain A in Fig. 2(b1)) forms two separated, U-shaped domains perpendicular to each other, and the vale bottoms of the U-domains occupy two poles of the nanorod. Therefore, the geometry of R$_4$ phase belongs to the same symmetry-group of a tennis ball or a horse saddle, D_{2d}, which means that if we reflect the morphology with respect to xy-plane, and rotate with respect to z-axis by $\pi/2$, then we get morphology that overlaps its original shape.

In the perpendicular (or ring-shaped) ripple phase, if one pole is covered by domain A, the other pole must be covered by domain B, and vice versa. The domain A or B itself only has rotational symmetry with respect to the cylinder axis, while the A and B combined morphology has D_∞ symmetry with inverted color.

The number of the ripple stripes in the cylinder region is determined by the competition between the stretching energy of polymer chains and the interfacial energy between different components. On one hand, since one end of each polymer is immobilized on the surface of the nanorod, the chains are extensively stretched out from their grafting point to reach their favorable domain area, leading to a stretching energy penalty. Therefore, a larger domain size causes higher stretching energy. On the other hand, increasing the stripe number

(which in turn decreasing the domain size) introduces more interfaces, and consequently increases the interfacial energy.

Note that a ripple structure perpendicular to the rod axis was also suggested for small molecule ligands by Singh *et al.*[15, 16] experimentally and theoretically. However, the reason of emergence of the perpendicular ripple phase in their work is different from our system: First, the radius of the curved substrate in their systems is much larger than their chain length, while in our case R is comparable to the radius of gyration of the polymer. The effect of the curvature of the substrate is much stronger in our systems; Second, the grafting point of the polymer in Ref. 15 is mobile on the substrate in the experiment as well as in DPD simulations, allowing macrophase separation. The emergence of perpendicular ripple phase in SCFT calculation of Egorov,[17] supporting the results of Singh *et al.*,[15, 16] is also due to the mobility of grafting sites. When the grafting sites are mobile, the interfacial energy can be decreased by increasing the width of the ripple stripes without any penalty of stretching energy. Therefore, the polymer prefers straight stripe domains oriented along the rod axis where the curvature is zero, rather than along the latitude direction where the curvature is the highest. Moreover, a rotational symmetry is enforced in Ref. 17, which makes the parallel ripple phase impossible.

2. The order parameter for polymer segregation

For the brushes immersed in a neutral solvent, the solvent penetrates into the brush region and dilute the polymers. At the A/B interface, due to the penetration of solvent, the probability of the contact between A and B segments is decreased, and consequently the width of the interface is increased as if the existence of solvent leads to a lower effective $\chi_{AB}N$. The strength of such phenomenon depends on the local curvature and the rod length. Therefore, in order to analyze the degree of segregation of polymer A and B, we define an order parameter $S(\mathbf{r})$ as

$$S(\mathbf{r}) = \sum_k \left(\phi_k(\mathbf{r}) - \overline{\phi_k(\mathbf{r})} \right)^2, \quad k = A, B, \quad (19)$$

where

$$\overline{\phi_k(\mathbf{r})} = \frac{N_k}{N_A + N_B} \left(\phi_A(\mathbf{r}) + \phi_B(\mathbf{r}) \right), \quad k = A, B \quad (20)$$

is the anticipated average density of component k. The order parameter S takes into account the sum of deviation of each component density, as well as the total polymer concentration $\phi_A(\mathbf{r}) + \phi_B(\mathbf{r})$ at position $\mathbf{r}$. The value of S vanishes either in the area where the polymer does not segregate, or where there is no polymer. The larger value of S indicates a stronger polymer segregation locally.

We take the symmetric brush-rod with R_4 structure as a typical example to analyze the behavior of the order parameter S, other ripple structures (either parallel or perpendicular) are similar. In R_4 structure, S in the equator plane $z = 0$ has an eightfold rotational symmetry with respect to the origin O (Fig. 3(a)). At the interface of A and B domains where the local volume fractions of A and B are equal, $S = 0$. At the positions far from the nanorod, where there are no polymers
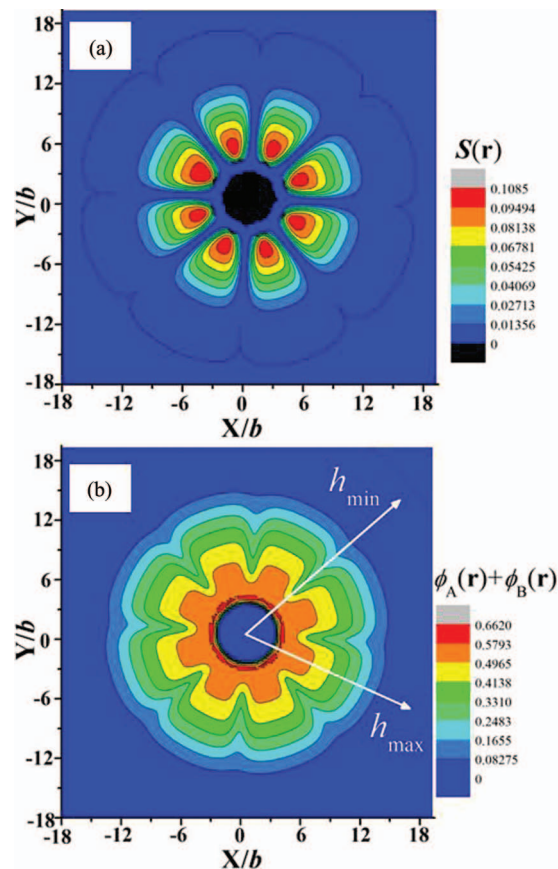

FIG. 3. (a) The value of the segregation order parameter $S(\mathbf{r})$ in the equator plane ($z = 0$) for the R_4 phase ($\chi_{AB}N = 40$) with $\varepsilon = 1.5$. (b) The total polymer density profile in the equator plane for with $\varepsilon = 3$. The h_{min} and h_{max} directions (white arrows) are the directions with the lowest and highest values of the brush height, respectively.

either, S also equals zero. The highest value of S occurs at the center line of each domain with a small distance to the grafting surface, since there is always a mixed layer of A and B above the core surface.

In order to compare the degree of segregation of mixed brushes with different elongation ϵ, we calculate the average $S(\delta)$ in the equator plane $z = 0$ with radius δ,

$$S(\delta) = \frac{\int_\delta S dl}{2\pi\delta}, \quad (21)$$

where $\int_\delta dl$ denotes the integration along the circle of radius $\delta = \sqrt{x^2 + y^2}$ in $z = 0$ plane. As shown in Fig. 4, $S = 0$ for $\delta < 3b$ and $\delta > 18b$, because the polymer density vanishes inside the nanorod core and far from the rod surface. The value of S is low in the grafting layer ($3b < \delta < 4b$). The uniform grafting density enforces the incompatible polymers to mix. Once the polymers leave the grafting area, they are stretched strongly to segregate into different domains, and S increases sharply and reaches its highest value within a distance of roughly $2b \sim 3b$ (in Fig. 4, the maximum of S is reached within a distance of $\delta = 6b \sim 7b$, this is because the rod here has a radius $R = 3b$ and δ is count from the center of the rod). Therefore, we conclude that the polymer chains need a thickness of $2b \sim 3b$ to overcome the influence of the uniform grafting. This thickness slightly increases when $\chi_{AB}N$
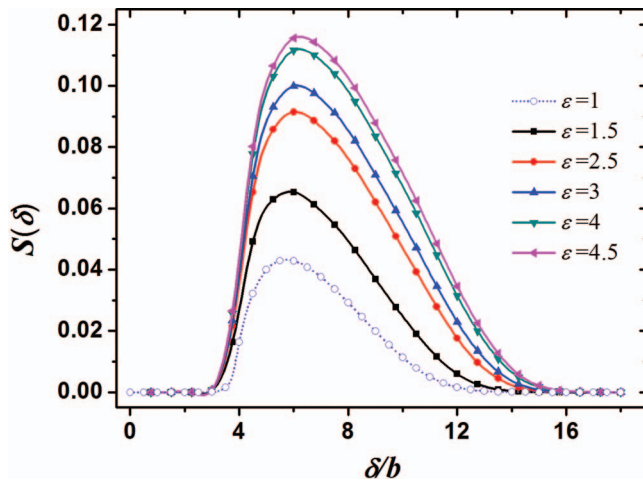
FIG. 4. The segregation order parameter S averaged along the circular lines of radius δ in the equator plane ($z = 0$) for the symmetric brush-rod systems ($\chi_{AB}N = 40$) with different ε (solid symbols with solid lines). The open circle with dotted line denotes S averaged over the sphere of radius δ of the spherical brush.

decreases to 20. Increasing δ further, S decreases smoothly, due to the decrease of total polymer concentration.

Comparing $S(\delta)$ of R$_4$ structure with different ε, we find that polymer segregation is systematically strengthened with increasing ε.

Note the large increase of S when we slightly elongate the spherical brush ($\varepsilon = 1$) to a short cylindrical brush ($\varepsilon = 1.5$). We interpret this phenomenon to the geometry difference of the substrate. According to simple scaling calculations,[3] the polymer density profile of a mono-component brush immersed in a neutral solvent decreases as r^{υ} where $\upsilon = -4/3$ for the star-like brush and $\upsilon = -2/3$ for the bottle-brush. Here, r is the radial distance to the center of the brush. Considering the same grafting density near the substrate, the faster decreasing rate of polymer density for the star-like brush than that for the cylindrical brush indicates that more solvents penetrate into the brush region for the star-like brush. Although the spherical brush and the cylindrical brush are far from the "infinitely thin substrate" limit, giving the same grafting density and radius R, we can confidently estimate the values of υ for a spherical brush and a cylindrical brush located in the crossover region that $-4/3 < \upsilon_{sphere} < \upsilon_{rod} < -2/3$. More solvents penetrate into the brush and dilute the polymer concentration, thus decrease the contribution of χ_{AB}. Hence, the segregation order parameter S, which decreases with decreasing total polymer density as well as with decreasing difference between ϕ_A and ϕ_B, exhibits large difference when the brush is slightly elongated (increasing ε by 0.5). Due to the same reason, S at the poles of a cylindrical brush is always much lower than that in the equator plane. Moreover, the density of the solvent is higher near A/B interface, as implied by lower $\phi_A + \phi_B$ at interface in Fig. 3(b), which further decreases the interfacial energy.

For $\varepsilon > 1$, since the radius R is kept constant, increasing ε refers to increasing the length of the cylindrical region, and consequently increasing the distance from the equator plane to the spherical caps of the nanorod. We attribute this mono-

tonically increasing S with ε to the decreasing influence of the poles. By increasing ε, S profile approaches to its value for the infinitely long cylindrical brush system, where the degree of polymer segregation is stronger than the finite cylindrical brushes. Although we are not able to carry out calculation for higher aspect ratio, we can conclude from Fig. 4 that beyond an ε value of 10, the S profiles represent those of an infinite long brush-rod system.

3. The height of symmetric brushes

Brush height, namely, the brush thickness, is a key character of polymer brushes, which is closely related to a series of physical properties such as the roughness of brush,[21] the interacting distance,[23, 27] and so forth.[3] Inspired by semi-dilute polymer brush studies,[13, 43] we define the height of the mixed polymer brushes as (here, we also take the symmetric brush-rod with R$_4$ structure as a typical example)

$$h = \frac{2 \int_0^L (\phi_A(\mathbf{r}) + \phi_B(\mathbf{r}))l\,dl}{\int_0^L (\phi_A(\mathbf{r}) + \phi_B(\mathbf{r}))\,dl}, \tag{22}$$

where $\int_0^L dl$ means the integration along a line l perpendicular to the nanorod surface, from $l = 0$ on the substrate to $l = L$ at the boundary of the simulation box where the polymer density is zero. The factor 2 in the numerator of the above equation is to ensure h corresponding to the correct brush height when the profile $\phi_A(\mathbf{r}) + \phi_B(\mathbf{r})$ takes a step-function-like shape with an exact thickness L.

The brush height depends on the polymer density profile on the integration contour. The distribution of total polymer density $\phi_A + \phi_B$ is not uniform in the space. According to the polymer density profile in the equator plane $z = 0$ (Fig. 3(b)), the maximum value of h occurs when the integration is along the center line of a domain (h_{max} in Fig. 3(b)), while the minimum value of h occurs when the integration is passing the interface of A and B domains (h_{min} in Fig. 3(b)). In our brush-rod system, the difference of h_{max} and h_{min} in the equator plane is about 5% of h_{max}.

The average brush height in the equator plane, denoted as $h_{equator}$, is always larger than the brush height at the poles, denoted as h_{pole} obtained by the integration of Eq. (22) along z-axis (Fig. 5). Both $h_{equator}$ and h_{pole} are greater than the average brush height for a spherical brush h_{sphere} with $\varepsilon = 1$ (Fig. 5). The difference between $h_{equator}$ and h_{pole} increases with ε, and $h_{equator}$ must go to a finite limit value for infinite long rod, although in our SCFT simulations the rod length H is not long enough to show the limit value.

An interesting phenomenon is that the ratio $h(Z)/h_{equator}$ shows very limited influence of $\chi_{AB}N$ despite the increasing height with $\chi_{AB}N$ (Fig. 6), where $h(Z)$ is the average brush height in the plane perpendicular to z-axis with distance Z to the origin O. For the rod with finite length, $h(Z)$ decreases from the equator to $Z = H/2$ where the cylinder region and the hemispherical cap is connected. The ratio $h(Z = H/2)/h_{equator}$ decreases from 0.99 to 0.92 when ε increases from 1.5 to 4.5. This phenomenon is consistent with the increasing difference between $h_{equator}$ and h_{pole} with increasing ε (Fig. 5). By further comparison with the brush height ratio for $\varepsilon = 4.5$ and
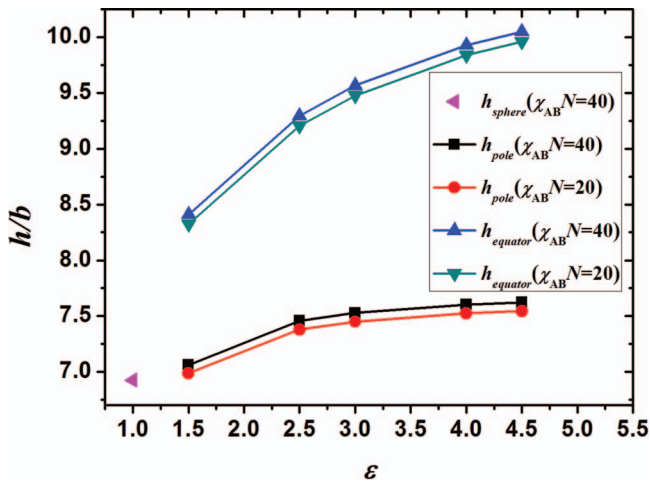
FIG. 5. The brush height at the poles h_{pole} and the average brush height in the equator plane $h_{equator}$ for the R_4 phase as a function of the aspect ratio ε of the nanorod. The pink triangle denotes the average brush height of the spherical brush of $\varepsilon = 1$ and $\chi_{AB}N = 40$.

$\chi_{AB}N = 0$, we conclude that in our brush system immersed in a neutral solvent, $\chi_{AB}N$ mainly influences the absolute value of the brush height, and has very slight influence on the relative height of $h(Z)/h_{equator}$. We surmise that a poor solvent or a selective solvent will lead to different brush height behavior. However, this is beyond the scope of the current paper.

Since our main focus in this paper is the effect of elongation of nanoparticles on brush morphology, we will not delve into the influence of the ratio of brush height to particle radius on the phase separation thermodynamics. Anyway, this is not a specific issue only for the present nanorod-brush system, it is also related to nanoparticle-brush systems with both isotropic (such as spherical brushes) and anisotropic (cylindrical brushes) shapes. We only point out that by changing the radius of the core of spherical mixed brushes, a variety of structures with different symmetries can be observed.[13]
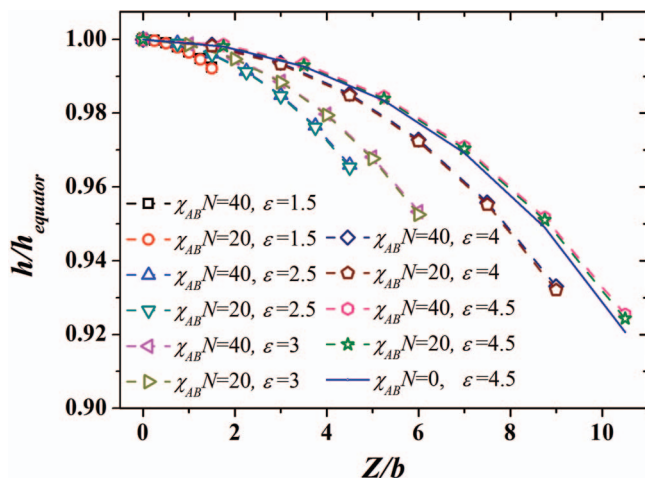
B. Asymmetric brushes

The asymmetric brush-rod systems here are defined as the mixed polymer brushes with either $N_A \neq N_B$ and/or $\sigma_A \neq \sigma_B$. The asymmetric parameters would introduce more complicated phase structures. To simplify the calculation, we keep $N_A + N_B$ and $\sigma_A + \sigma_B$ constant, and systematically change $N_A/(N_A + N_B)$, $\sigma_A/(\sigma_A + \sigma_B)$, and ε to observe the evolution of phase separated morphology.

Similar as for symmetric brushes, asymmetric brushes can be fabricated experimentally by controlling the polymerization of different species,[44–46] changing the ratio of two initiators on the substrate, etc.

1. $\sigma_A \neq \sigma_B$ and $N_A = N_B$

For spherical cases ($\varepsilon = 1$), using SCFT, Roan[12] predicted that by increasing the chain number difference of two components (corresponding to the grafting density difference), a spherical brush exhibits a sequence of ripple phase, sphere/island phase, and layer phase. Such a sequence was also validated in our previous work.[13]

We denote the ripple phase as Ripple, the ring-shaped phase as n-Rin, the sphere phase as S without regarding the number of spherical domains, and the layer phase as L_{BA} where the minor component B forms the outer layer and the major component A forms the core (Fig. 7(a)). In this work, although the grafting density and the chain length are not the same, the region of Ripple, S, and L_{BA} phase is consistent with the result reported by Roan in Ref. 12. For the spherical brush, Ripple, S, and L_{BA} phase locate at $0.5 < f_A < 0.62$, $0.62 < f_A < 0.83$, and $f_A > 0.83$, respectively, while they locate at $f_A = 0.5$, $f_A = 0.75$, and $f_A > 0.833$ for $N_A = N_B = 20$ in Ref. 12, respectively. For the cases of cylindrical brushes ($\varepsilon > 1$), besides Ripple, S, and L_{BA}, the ring-shaped phase (denoted as n-Rin) emerges between the region of Ripple and S.

FIG. 6. The ratio of brush height $h(Z)/h_{equator}$ for the R_n phase with different $\chi_{AB}N$, where $h(Z)$ is the average brush height in the plane $z = Z$ and $h_{equator} = h(0)$.
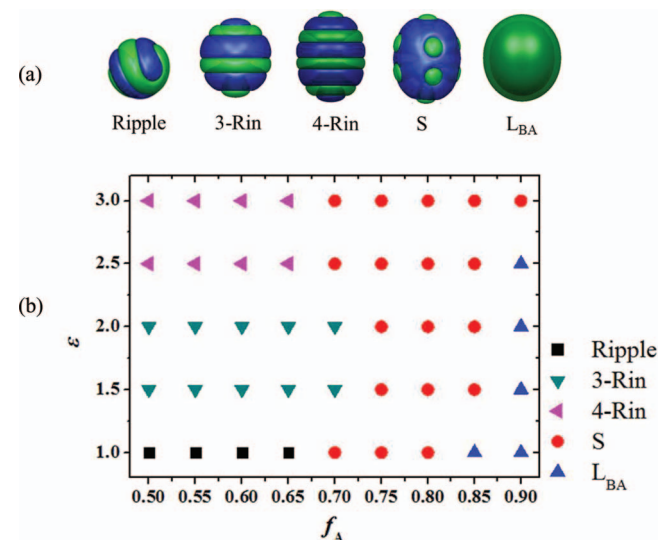

FIG. 7. (a) Morphologies of typical structures of the asymmetric brush-rod system ($\chi_{AB}N = 40$) with $N_A = N_B = 24$ and $\sigma_A \neq \sigma_B$. (b) The phase diagram of the asymmetric brush-rod in terms of ε and $f_A = \sigma_A/(\sigma_A + \sigma_B)$.

Note that the domains of the minor component always emerge on the surface of the brush, even though its relative volume fraction $f_B = 1 - f_A$ reaches a small value of 0.1. We ascribe this to the different entropy contributions even with the same chain length of A and B. Indeed, for $\varepsilon = 1.5$ in Fig. 7(a), the enthalpic contribution (per unit volume) from the A (majority) and B chains are 0.00107374, and the entropy contributions from the A and B chains are -0.01156591 and -0.00150288, respectively. It is clear that the entropy change of the A chains is more important in determining the morphology and the system prefers not to stretch the A chains too much. However, if B domain was embedded in domain A, e.g., forming a phase L_{AB} composed of a domain A shell and a domain B core, the A chains have to be stretched further away from the substrate, leading to a significantly stronger entropy penalty than that of A core and B shell, which is a L_{BA} phase. In fact, only if $N_B \ll N_A$, as shown in Sec. III B 2, the interfacial energy overcomes the entropy penalty of the short chain and L_{AB} becomes stable.

In the phase diagram (Fig. 7(b)), ring-shaped phase (3-Rin and 4-Rin) for brush-rods ($\varepsilon > 1$) replaces Ripple phase for the spherical brush when $f_A < 0.7$. Further increasing f_A, S phase becomes stable. The stable area of S phase in the phase diagram increases with ε so fast that for $\varepsilon = 3$ the highest f_A value to obtain S reaches 0.9. This volume fraction already corresponds to L_{BA} phase for spherical brushes.

Due to the increasing stable region of S phase, the region of L_{BA} shrinks with increasing ε (Fig. 7(b)). For $f_A = 0.9$, L_{BA} only emerges for $\varepsilon < 2.5$ and S phase substitutes for $\varepsilon \geq 2.5$. For $f_A = 0.9$ and $\varepsilon = 4.5$, which is not drawn in Fig. 7(b), ripple structure emerges in the cylinder region of the brush while the islands at the poles disappear. Note that this ripple structure has the same symmetric group D_{2h} as S shown in Fig. 7(a).

In conclusion, when the chain lengths for A and B polymers are the same, the stable region of ring-shaped and S structures increase rapidly with increasing ε. However, limited by the parameter space we searched at the moment, we cannot conclude that the ripple structure is always stable for the infinitely long cylindrical brushes with asymmetric grafting density.

2. $\sigma_A = \sigma_B$ and $N_A \neq N_B$

We keep the grafting density $\sigma_A = \sigma_B = 0.3b^{-2}$, and change the chain length of A, B polymers. Therefore, the relative volume fraction of component A is $f_A = N_A/(N_A + N_B)$.

We choose $\varepsilon = 3$ and change the chain length, and illustrate the microdomain configuration for different f_A as shown in Fig. 8. Other choice of ε leads to qualitatively similar microdomain configurations. Comparing with the phase sequence for $\varepsilon = 3$ in the phase diagram for $N_A = N_B$ (Fig. 7(b)), S phase never exists for non-equal chain length, while the period number of the ripple structures shows a tendency to increase when chain length difference increases. Note that the number n for R_n here is determined by the domains of the minor component. Therefore, even when the domain of B polymer is embedded in domain A, we still classify
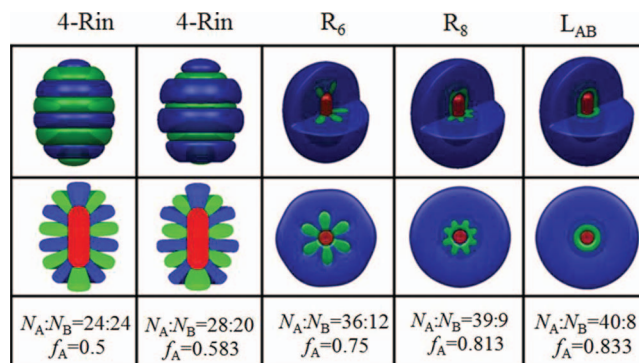

FIG. 8. The morphologies of the asymmetric brush-rod systems ($\chi_{AB}N = 40$) with $\sigma_A = \sigma_B = 0.3b^{-2}$ and $N_A \neq N_B$. The relative volume fraction $f_A = N_A/(N_A + N_B)$, where $N_A + N_B = 48$ and $\varepsilon = 3$. The lower row shows the cross section of the corresponding morphologies in the upper row in the plane that includes the z-axis or in the equator plane $z = 0$. The blue, green, and red regions correspond to domain A, domain B, and the nanorod, respectively.

it as the ripple phase to emphasize that the undulation of A/B interface is parallel to the rod axis. Nevertheless, the definition of the ripple structure is optional to a certain extent, e.g., R_8 structure connecting R and L_{AB} in Fig. 8 can also be considered as L_{AB} structure with undulating interface.

The period number n for the ripple phase increases from four to eight when the chain length difference increases (Fig. 8). Since $N_A + N_B$ is fixed, increasing chain length difference leads to the increasing difference of the radius of gyration of A and B polymers. The longer chains (polymer A in Fig. 8) extend farther into the solvent, and always have more free space than the shorter chains (polymer B in Fig. 8) to balance the entropic penalty for the strong stretching near the substrate. Therefore, the length of the shorter chains determines the phase structure in short distance from the grafting substrate. The domain size close to the radius of gyration of the shorter chain is always preferable. The shorter is the polymer B chain, the smaller is the size of B domains, and correspondingly the larger ripple period numbers. However, when the chain for the minor component is too short ($N_A \leq 8$, i.e., $f_B \leq 0.17$), a layer phase L_{AB} composed of a small core of B domain and a thick shell of A domain emerges, which minimizes the interfacial energy with a little expense of the stretching energy of chain A.

By changing the Flory-Huggins parameter χ_{AB}, we find that the transition from L_{AB} to R_n depends on the chemical incompatibility of the two components. We choose the lengths $N_A = 34$ and $N_B = 14$, the parameters corresponding to L_{AB} phase for spherical brush, and systematically change $\chi_{AB}N$ from 20 to 40 with different ε (Fig. 9). The ripple phase R_n only exists for $\chi_{AB}N \geq 35$ and $\varepsilon \geq 2$. When χ_{AB} increases, the mixed polymer layer, which is the domain near the substrate, tends to shrink to decrease the energy caused by the contacting of A and B segments. Therefore, L_{AB} structure is not stable for large χ_{AB}, because the incompatibility drives A chain out of B domain, inducing the undulation of A/B interface, and consequently leads to the ripple structure. By closely looking into the details of the density profile near the transition point between R_6 and L_{AB} in Fig. 9, we find L_{AB}
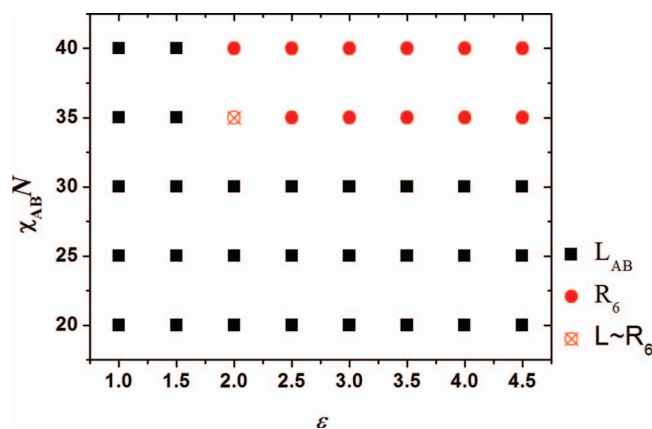
FIG. 9. Phase diagram of the asymmetric brush-rod systems with $\sigma_A = \sigma_B = 0.3b^{-2}$, $N_A = 34$, and $N_B = 14$. The symbol ⊠ means that the free energy difference of L and R_6 phases is not distinguishable by our SCFT calculation.

structure near both poles of the brush, while in the rod region of the brush there exists R_6 phase. This is because of the stronger solvent penetration leading to a weaker segregation near the poles of the brush.

Other than the Flory-Huggins parameter and chain length difference, the particle anisotropy (in the nanorod case the aspect ratio ε) also plays an important role in changing the morphology of the asymmetric brushes (Fig. 9). For (nearly) spherical nanoparticles, there is a relatively larger outer space for A and B chains, which reduces their unfavorable contacts, therefore a L_{AB} can exist. As ε exceeds 2 for higher $\chi_{AB}N$ values, a transition from L_{AB} to R_n occurs due to less space for A and B chains in the rod region than near the poles (with more space), i.e., there would be too many unfavorable contacts between A and B segments in the rod region if they mixed together.

IV. CONCLUSIONS

By using SCFT combined with the masking technique, we studied the phase structures of binary mixed brush-rod systems. The brush composed of two chemically distinct polymers A and B is uniformly grafted on the surface of a nanorod, and the system is immersed in a nonselective neutral solvent. We focus on the morphology of phase separation in the brush, and study its response to a series of parameters, such as the aspect ratio of the nanorod ε, the grafting densities σ_A and σ_B, and the chain lengths N_A and N_B.

The symmetric brush-rod system, defined as $N_A = N_B$ and $\sigma_A = \sigma_B$, is found to prefer either perpendicular or parallel ripple phase. According to the order parameter for polymer segregation, we conclude that larger substrate curvature causes a stronger penetration of the solvent, and hence leads to a weakened segregation due to the dilution of polymer density especially near the interface between A and B domains. The height of the brush varies from its highest value in equator plane to the lowest value at poles. Although the brush height itself increases with increasing Flory-Huggins parameter $\chi_{AB}N$, the height ratio $h/h_{equator}$ along the latitude line depends only on ε, while $\chi_{AB}N$ has very limited influence.

The asymmetric brush-rod systems are categorized into two types. For brushes with equal chain length ($N_A = N_B$) and non-equal grafting density ($\sigma_A \neq \sigma_B$), in the phase diagram when the aspect ratio of the nanorod ε increases, the stable region of the ripple and sphere phase increases rapidly, and consequently the stable regions of the layer phase shrinks. For asymmetric brushes with equal grafting density ($\sigma_A = \sigma_B$) and non-equal chain length ($N_A \neq N_B$), the parallel ripple phase is more stable in the phase diagram at high ε and $\chi_{AB}N$ values, and the layer phase dominates when both the chain length difference is sufficiently high and $\chi_{AB}N$ is low.

In this paper, we consider the binary mixed brush-rod system with finite rod length, which bridges the properties of spherical brushes and infinitely long cylindrical brushes. To simplify the analysis, only neutral solvent is considered at present. However, the influence of selective solvent, which has already been widely noticed in experiments, remains an interesting topic that requires more efforts to study. We note that it is straightforward to extend the present model to this complicated yet still realistic situation. The findings may have various implications for creating novel polymeric nanocomposites.

[1]N. Ayres, Polym. Chem. **1**, 769 (2010).
[2]R. C. Advincula, W. J. Britlain, and K. C. Caster, in *Polymer Brushes*, edited by J. Rühe (Wiley-VCH, Weinheim, 2004).
[3]K. Binder and A. Milchev, J. Polym. Sci., Part B: Polym. Phys. **50**, 1515 (2012).
[4]B. Zhao and W. J. Brittain, Prog. Polym. Sci. **25**, 677 (2000).
[5]B. Zhao and L. Zhu, Macromolecules **42**, 9369 (2009).
[6]E. Zhulina and A. C. Balazs, Macromolecules **29**, 2667 (1996).
[7]S. Minko, M. Müller, D. Usov, A. Scholl, C. Froeck, and M. Stamm, Phys. Rev. Lett. **88**, 035502 (2002).
[8]A. Sidorenko, S. Minko, K. Schenk-Meuser, H. Duschner, and M. Stamm, Langmuir **15**, 8349 (1999).
[9]B. Zhao, R. T. Haasch, and S. MacLaren, J. Am. Chem. Soc. **126**, 6124 (2004).
[10]L. Zhu and B. Zhao, J. Phys. Chem. B **112**, 11529 (2008).
[11]J.-R. Roan, Int. J. Mod. Phys. B **18**, 2469 (2004).
[12]J.-R. Roan, Phys. Rev. Lett. **96**, 248301 (2006).
[13]Y. Q. Wang, G. A. Yang, P. Tang, F. Qiu, Y. L. Yang, and L. Zhu, J. Chem. Phys. **134**, 134903 (2011).
[14]E. B. Zhulina, C. Singh, and A. C. Balazs, Macromolecules **29**, 6338 (1996).
[15]C. Singh, Y. Hu, B. P. Khanal, E. R. Zubarev, F. Stellacci, and S. C. Glotzer, Nanoscale **3**, 3244 (2011).
[16]C. Singh, A. M. Jackson, F. Stellacci, and S. C. Glotzer, J. Am. Chem. Soc. **131**, 16377 (2009).
[17]S. A. Egorov, Soft Matter **8**, 3971 (2012).
[18]J. F. Marko and T. A. Witten, Phys. Rev. Lett. **66**, 1541 (1991).
[19]J. F. Marko and T. A. Witten, Macromolecules **25**, 296 (1992).
[20]B. Zhao and W. J. Brittain, Macromolecules **33**, 8813 (2000).
[21]J. M. Horton, S. D. Tang, C. H. Bao, P. Tang, F. Qiu, L. Zhu, and B. Zhao, ACS Macro Lett. **1**, 1061 (2012).

[22]B. Zhao and T. He, Macromolecules **36**, 8599 (2003).

[23]S. A. Egorov, J. Chem. Phys. **129**, 064901 (2008).

[24]D. Meng and Q. Wang, J. Chem. Phys. **130**, 134904 (2009).

[25]M. Müller, Phys. Rev. E **65**, 030802 (2002).

[26]S. A. Egorov, J. Chem. Phys. **137**, 134905 (2012).

[27]J. U. Kim and M. W. Matsen, Macromolecules **41**, 4435 (2008).

[28]B. Zhao and L. Zhu, J. Am. Chem. Soc. **128**, 4574 (2006).

[29]M. J. Mulvihill, B. L. Rupert, R. He, A. Hochbaum, J. Arnold, and P. Yang, J. Am. Chem. Soc. **127**, 16040 (2005).

[30]H. P. Hsu, W. Paul, and K. Binder, Macromol. Theory Simul. **16**, 660 (2007).

[31]S. Alexander, J. Phys. (Paris) **38**, 983 (1977).

[32]M. Daoud and J. P. Coton, J. Phys. (Paris) **43**, 531 (1982).

[33]D. I. Dimitrov, A. Milchev, and K. Binder, J. Chem. Phys. **127**, 084905 (2007).

[34]J. F. Li, J. Fan, H. D. Zhang, F. Qiu, P. Tang, and Y. L. Yang, Eur. Phys. J. E **20**, 449 (2006).

[35]G. Yang, P. Tang, Y. L. Yang, and J. T. Cabral, J. Phys. Chem. B **113**, 14052 (2009).

[36]M. W. Matsen and M. Schick, Phys. Rev. Lett. **72**, 2660 (1994).

[37]F. Drolet and G. H. Fredrickson, Phys. Rev. Lett. **83**, 4317 (1999).

[38]Z. Guo, G. Zhang, F. Qiu, H. Zhang, Y. Yang, and A.-C. Shi, Phys. Rev. Lett. **101**, 028301 (2008).

[39]Q. Wang, T. Taniguchi, and G. H. Fredrickson, J. Phys. Chem. B **108**, 6733 (2004).

[40]V. Khanna, E. W. Cochran, A. Hexemer, G. E. Stein, G. H. Fredrickson, E. J. Kramer, X. Li, J. Wang, and S. F. Hahn, Macromolecules **39**, 9346 (2006).

[41]G. Tzeremes, K. Ø. Rasmussen, T. Lookman, and A. Saxena, Phys. Rev. E **65**, 041806 (2002).

[42]A. Bueno-Orovio, V. M. Pérez-García, and F. H. Fenton, SIAM J. Sci. Comput. **28**, 886 (2006).

[43]D. Dukes, Y. Li, S. Lewis, B. Benicewicz, L. Schadler, and S. K. Kumar, Macromolecules **43**, 1564 (2010).

[44]X. M. Jiang, G. J. Zhong, J. M. Horton, N. X. Jin, L. Zhu, and B. Zhao, Macromolecules **43**, 5387 (2010).

[45]X. M. Jiang, B. Zhao, G. J. Zhong, N. X. Jin, J. M. Horton, L. Zhu, R. S. Hafner, and T. P. Lodge, Macromolecules **43**, 8209 (2010).

[46]C. H. Bao, S. D. Tang, J. M. Horton, X. M. Jiang, P. Tang, F. Qiu, L. Zhu, and B. Zhao, Macromolecules **45**, 8027 (2012).